Behavioral/Systems/Cognitive

Deep and Superficial Amygdala Nuclei Projections Revealed *In Vivo* by Probabilistic Tractography

Dominik R. Bach,[1] Timothy E. Behrens,[1] Lúcia Garrido,[2] Nikolaus Weiskopf,[1] and Raymond J. Dolan[1]

[1]Wellcome Trust Centre for Neuroimaging and [2]Institute of Cognitive Neuroscience, University College London, London WC1N 3BG, United Kingdom

Despite a homogenous macroscopic appearance on magnetic resonance images, subregions of the amygdala express distinct functional profiles as well as corresponding differences in connectivity. In particular, histological analysis shows stronger connections for superficial (i.e., centromedial and cortical), compared with deep (i.e., basolateral and other), amygdala nuclei to lateral orbitofrontal cortex and stronger connections of deep compared with superficial, nuclei to polymodal areas in the temporal pole. Here, we use diffusion weighted imaging with probabilistic tractography to investigate these connections in humans. We use a data-driven approach to segment the amygdala into two subregions using *k*-means clustering. The identified subregions are spatially contiguous and their location corresponds to deep and superficial nuclear groups. Quantification of the connection strength between these amygdala clusters and individual target regions corresponds to qualitative histological findings in non-human primates, indicating such findings can be extrapolated to humans. We propose that connectivity profiles provide a potentially powerful approach for *in vivo* amygdala parcellation and can serve as a guide in studies that exploit functional and anatomical neuroimaging.

Introduction

The amygdala is a gray matter collection of nuclei situated in anterior temporal lobes, rostral to hippocampus and ventromedial to the striatum (McDonald, 1998). The amygdala is implicated in a range of behavioral functions that span relevance detection (Sander et al., 2003; Zald, 2003), face perception (Adolphs and Spezio, 2006), autonomic expression of emotion (Davis and Whalen, 2001), and value learning (LeDoux, 2000). This functional diversity is mirrored in the complexity of its internal structure which subsumes >20 different nuclei, based on histological criteria (Freese and Amaral, 2009). These subdivisions can be broadly parcellated into a deep group, encompassing the lateral, basal, and smaller nuclei, and a superficial group, consisting of central, medial, and cortical nuclei (Pitkänen, 2000).

In aversive learning and the autonomic expression of emotion, different functions are ascribed to these two groups. In rodent experiments, deep nuclei are implicated in establishing a stimulus/response association, while the centromedial group is considered a relay for generating learning-based autonomic and behavioral outputs (LeDoux, 2000) as well as other emotional responses (Gray and McNaughton, 2000). Paralleling this functional segregation, the two groups also differ in their profile of afferent/efferent cortical connections (Carmichael and Price, 1995; McDonald, 1998; Pitkänen, 2000), most notably with respect to connections to polymodal area TG in the temporal pole lateral (TP) and the lateral orbitofrontal cortex (OFC), respectively. More specifically, the temporal pole sends strong projections to lateral and accessory basal nuclei and light projections to the basal nucleus which are all situated in the deep group. By contrast, the lateral OFC has extensive connections to all superficial nuclei, and only to small parts of the lateral (i.e., dorsal portion) and basal (i.e., magnocellular subdivision) nuclei.

Here, we sought to investigate these distinct projections *in vivo* using diffusion imaging and probabilistic tractography. Diffusion imaging characterizes the apparent diffusion properties of water (Basser et al., 1994a,b). In the brain's white matter, the principal diffusion direction corresponds to the orientation of major fibers in each voxel (Beaulieu and Allen, 1994). Local diffusion properties can be followed through space using probabilistic tractography to reconstruct large fiber tracts (Behrens et al., 2003a). Thus, in principle one can infer the connections from each point in the amygdala to the cortex.

In the absence of an established method to parcellate individual amygdala nuclei on magnetic resonance images, we used a clustering method as a data-driven approach to identify amygdala regions with unique connectivity profiles. Note this algorithm is blind to the spatial position of cortical targets and therefore blind to our core hypotheses. We predicted we would find two amygdala regions that differ in the density of connections to OFC/TP in a manner consistent with *in vitro* histological studies, and that these locations would correspond to superficial and deep nucleus group. We developed our methods on a first dataset and then acquired a second new dataset, with higher quality images, so as to independently confirm our results.

Materials and Methods

Data acquisition and preprocessing. We acquired diffusion-weighted images from a group of 16 healthy right-handed individuals (6 men/10 women, mean age ± SD 29.4 ± 5.8 years) and a completely independent

Received May 28, 2010; revised Sept. 22, 2010; accepted Oct. 25, 2010.

This work was funded by a Wellcome Trust Programme Grant to R.J.D., a Max Planck Research Award to R.J.D., and a personal grant from the Swiss National Science Foundation to D.R.B. We thank Zoltan Nagy and Saad Jbabdi for support.

Correspondence should be addressed to Dominik R. Bach, Wellcome Trust Centre for Neuroimaging, 12 Queen Square, London WC1N 3BG, UK. E-mail: d.bach@fil.ion.ucl.ac.uk.

DOI:10.1523/JNEUROSCI.2744-10.2011

 0270-6474/11/310618-06$15.00/0

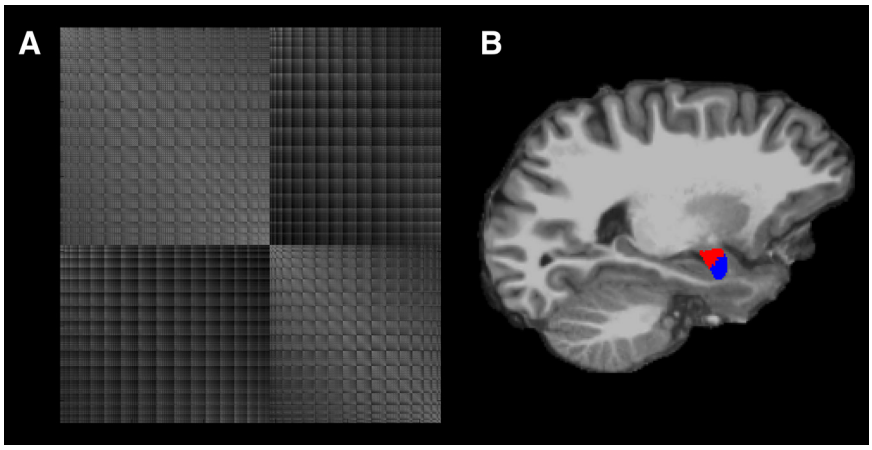

Figure 1. Illustration of the clustering method on data from an individual participant. ***A***, Reordered cross-correlation matrix after *k*-means clustering with $k = 2$ clusters. ***B***, Sagittal view of resulting clusters shows spatial contiguity and localization in accordance with a deep/superficial segmentation.

group of 8 healthy right-handed individuals for replication (2 men/6 women, mean age ± SD, 23.8 ± 3.7 years), subsequently referred to as dataset 1 and 2. All participants gave written informed consent, and the study was approved by the local ethics committee.

The experiments were performed on a 3T whole-body MRI scanner (Magnetom Tim Trio, Siemens Healthcare) operated with an RF body transmit and 12-channel (dataset 1) or 32-channel (dataset 2) receive head coil. Diffusion weighted images were acquired using a spin-echo echoplanar imaging (EPI) sequence, with twice refocused diffusion-encoding to reduce eddy-current-induced distortions (Reese et al., 2003). Amplitudes of diffusion-encoding gradients were calibrated for unbiased measurement of diffusion directions and improved fiber tracking (Nagy et al., 2007). We acquired 60 axial slices in interleaved order [2.3 mm isotropic resolution; image matrix = 96 × 96, field of view = 220 × 220 mm^2, slice thickness = 2.3 mm with no gap between slices, repetition time (TR) = 9.0 s (dataset 1) and 8.4 s (dataset 2), echo time (TE) = 90 ms, asymmetric echo shifted forward by 24 phase-encoding (PE) lines, readout bandwidth (BW) = 2003 Hz/pixel] for 68 images with unique diffusion encoding directions. The first seven reference images were acquired with a *b*-value of 100 s/mm^2, the remaining 61 images with a *b*-value of 1000 s/mm^2 (Nagy et al., 2007). EPI images suffer from susceptibility-induced geometric distortions, particularly in basal brain regions. To minimize these distortions, two sets of 68 images were collected during each scan with opposite PE gradient polarity. To correct for head motion, images within each of the two acquisitions were aligned to a synthetic reference (Chang et al., 2005) using standard procedures in Camino (http://www.cs.ucl.ac.uk/research/medic/camino/). The two datasets were then combined to estimate the local magnetic fields and correct the images using a method which exploits the fact that images with opposite PE polarity show exactly opposite distortions (Andersson et al., 2003). To enhance signal-to-noise in dataset 2, the two image sets were acquired twice and averaged after correction for motion, before distortion correction.

Anatomical T1-weighted images were acquired in each participant using a modified driven equilibrium Fourier transform (MDEFT) sequence with optimized parameters as described previously (Deichmann et al., 2004). For dataset 1, 176 sagittal partitions were acquired with an image matrix of 256 × 240 (read × phase) and twofold oversampling in read direction (head/foot direction) to prevent aliasing (1 mm isotropic spatial resolution, excitation flip angle $\alpha = 16°$, TR/TE/inversion time = 7.92 ms/2.48 ms/910 ms, BW = 195 Hz/pixel). In dataset 2, we used an MDEFT sequence with similar parameters but higher resolution (0.77 mm isotropic spatial resolution, 224 sagittal partitions, image matrix = 304 × 288, BW = 196 Hz/pixel). This sequence was acquired twice, and the two images were coregistered and averaged offline using SPM8 functions (http://www.fil.ion.ucl.ac.uk/spm). For both types of acquisitions, composite RF excitation pulses were used to compensate for $B1^+$/RF transmit field inhomogeneities (Deichmann et al., 2002). Fat suppression was used to reduce scalp signal and ringing artifacts due to head motion (Howarth et al., 2006). Images were reconstructed by performing a standard 3D Fourier transform, followed by modulus calculation. No data filtering was applied in *k*-space or in the image domain.

Seed region definition. To provide an accurate definition of the seed region, the amygdala was manually delineated on T1-weighted images using Anatomist (www.brainvisa.info). The inferior/posterior and anterior/superior boundary, in general clearly visible on at least a few sagittal slices, were marked: the most posterior point were the posterior nuclei border the ventral horn of the anterior extent of the lateral (temporal) ventricle and white matter; the inferior boundary separating amygdala from hippocampus and lateral ventricle; the anterior boundary separating amygdala from white matter, entorhinal cortex, gyrus ambiens and uncus. We then proceeded from posterior to anterior in coronal slices (see supplemental Fig. S1 *A–C*, available at www.jneurosci.org as supplemental material), using the sagittally marked boundaries, the hippocampus, the optical tract, and the sulcus semiannularis as guiding landmarks. Each slice was compared against schematic tables of an anatomical atlas (Mai et al., 2008). Particular care was taken not to include the peduncle of the lentiform nucleus, hippocampal tissue, and periamygdaloid tissue between lateral amygdala and white matter of the temporal lobe. Amygdala boundaries were then straightened in sagittal slices, and once more controlled in coronal slices. Seed mask boundaries were automatically smoothed, using the SPM8 functions *spm_erode* and *spm_dilate* (see supplemental Fig. S1 *D*, *E*, available at www.jneurosci.org as supplemental material). Mean volume ± SD of the seed masks was 1356 ± 209 mm^3 for dataset 1, and 1048 ± 217 mm^3 for dataset 2, thus indicating a conservative definition of this structure (Zald, 2003).

Target region definition. Target masks were provided by automatic cortical parcellation of T1-weighted images using Freesurfer (version 4.1 for dataset 1; version 4.5 for dataset 2; http://surfer.nmr.mgh.harvard.edu/) in a standard processing stream that included Talairach registration, skull stripping (Ségonne et al., 2004), segmentation of gray and white matter (Dale et al., 1999; Fischl et al., 1999), and probabilistic labeling of cortical structures (Fischl et al., 2004). To account for parcellation inaccuracies and the lower resolution of the diffusion data, masks for the lateral OFC and TP were each dilated by 5 mm into every direction using the FSL function *fslmaths* (see an example for the final masks in supplemental Fig. S2, available at www.jneurosci.org as supplemental material). Both masks were then combined, and the overlap subtracted. The individual target subregion masks were used for *post hoc* analysis.

Probabilistic tractography. The FMRIB Software Library (FSL) (version 4.1.4 for dataset 1; version 4.1.2 for dataset 2; www.fmrib.ox.ac.uk/fsl) was used for tractography. Skull-stripped reference diffusion images were coregistered to skull-stripped T1-weighted images using FLIRT, and the inverse transformation was used to transform seed and target masks into diffusion space. All tractography was done in diffusion space, and the results were transformed back to T1-weighted masks for post-processing and display. We calculated probability distributions on two fiber directions at each voxel using a multiple fiber extension (Behrens et al., 2007) of a previously published diffusion modeling approach (Behrens et al., 2003a,b). Drawing on these distributions, we estimated fiber tracts between seed and ipsilateral target region. This approach draws a sample from each fiber orientation distribution at the current voxel and chooses the sample closest to the orientation of its previous step. The connection probability between a seed and any other voxel in the brain is given by the number of traces arriving at the target site. To suppress tracts that reached the target indirectly via alternative amygdala projections, we used the thalamus, brainstem and bilateral target as a termination mask

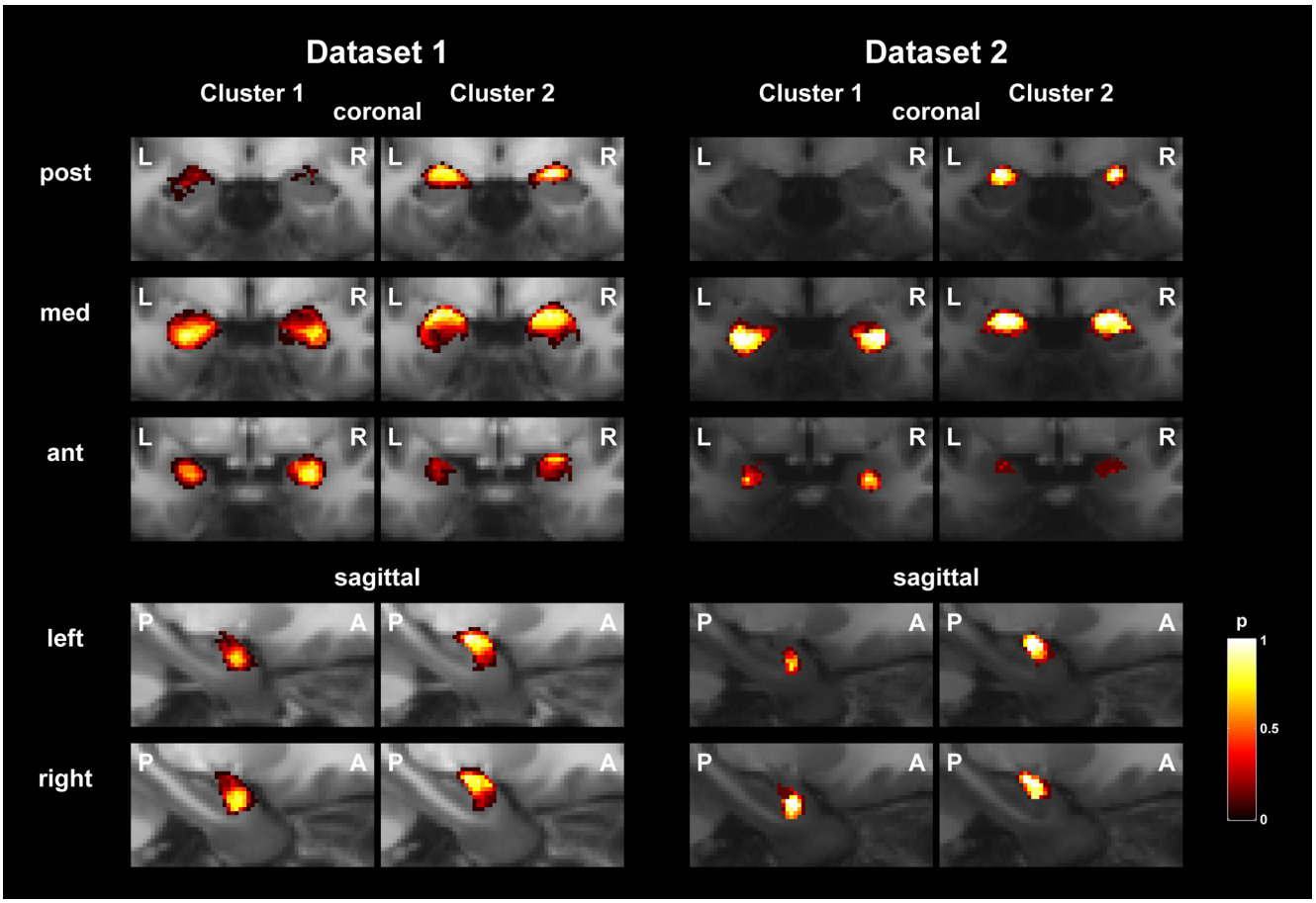

Figure 2. Group probability maps for the two clusters and two datasets in dataset-specific DARTEL space.

(stop mask), i.e., every trace was stopped once it exited the termination mask. Because some parts of the amygdala have a larger physical distance from the target mask than others, these would have higher overall connection likelihood with the whole target, and this could possibly bias the clustering algorithm used for automated parcellation. Hence, we corrected probability counts by the length of the pathway, as described previously (Tomassini et al., 2007). This approach gives greater weight to longer connections and penalizes short ones. To analyze connections from the resulting amygdala subregions to the target regions, we were interested in absolute measures of connectivity and did not correct for distance.

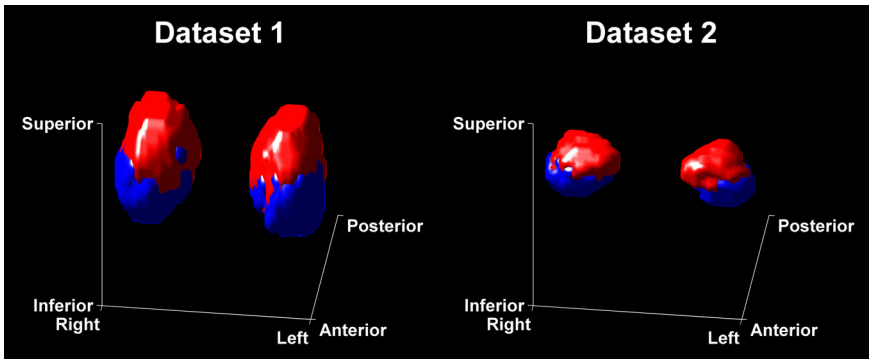

Figure 3. Three-dimensional rendering of group maximum probability maps in dataset-specific DARTEL space, thresholded at $p = 0.3$ and seen from a frontal, slightly elevated angle. The deep cluster 1 is shown in blue, and the superficial cluster 2 in red.

Automated parcellation. Cross-correlation between the connectivity patterns of all voxels in the seed mask were calculated and used for automatic parcellation (Johansen-Berg et al., 2004; Behrens and Johansen-Berg, 2005). The cross-correlation matrix was fed into *k*-means segmentation for automated clustering using an algorithm published in Hartigan (1975). Two hundred iterations with a predetermined number of two clusters were performed, resulting in two subsets of seed voxels. This approach minimizes the mean squared difference of each cluster's elements from its centroid, while maximizing the squared difference between cluster centroids (see Fig. 1A for an example of a reordered cross correlation matrix). For final analysis, seed voxel location was taken into account for *k*-means clustering to ensure contiguous voxel clusters. The algorithm is, however, completely blind to target voxel location, and therefore unbiased in relation to our hypotheses. The initial cluster assignments were randomly determined. To exclude a possibility that the initialization influences the clustering solution, we randomly chose three amygdalae from different individuals and repeated the clustering 1000 times with different random initial cluster assignments. The resulting assignment was congruent across all 1000 repetitions for 99.97%, 100%, and 100% of the voxels, for the three amygdalae, respectively. This shows that in our datasets clustering is independent of the starting points.

Between-subject alignment. For display purposes alone, all T1-weighted images from each dataset were brought into a common space using DARTEL (Ashburner, 2007) in SPM8 which allows for improved between-subjects alignment. Based on the estimated deformations, cluster images were then brought into the same space, and overlaid to provide group probability maps.

Statistical analysis. Probabilistic tractography measures the likelihood of connection between each voxel in each of the two amygdala subregions

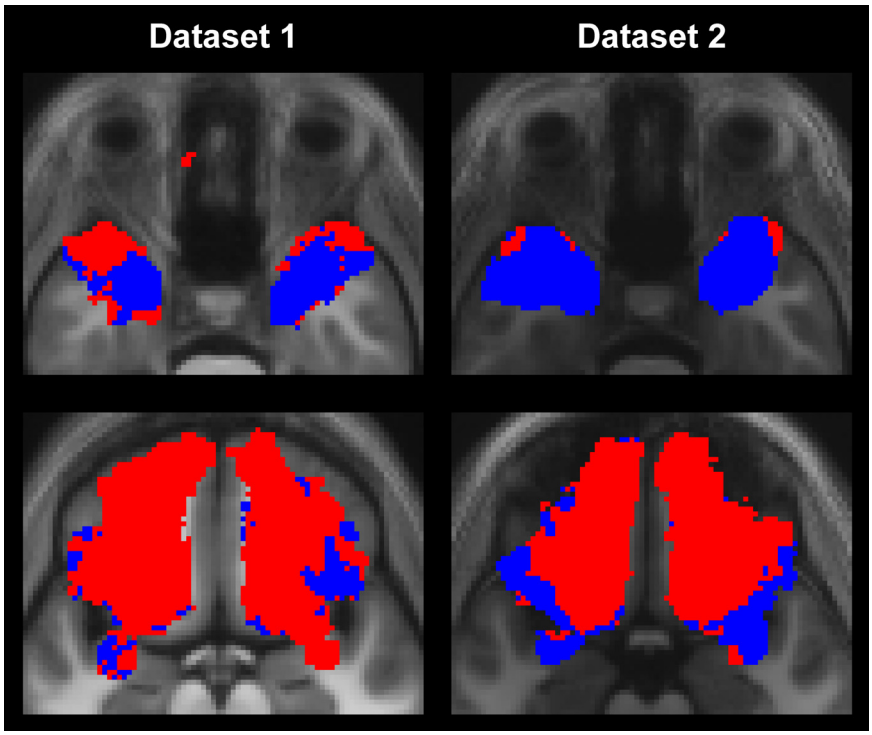

Figure 4. Group maximum probability maps of binary images that indicate whether any target voxel had relatively stronger connections to one or the other seed cluster, as determined by the clustering algorithm. Target voxels that have stronger connections to the deep cluster 1 are shown in blue; target voxels that connect more strongly to the superficial cluster 2 are red.

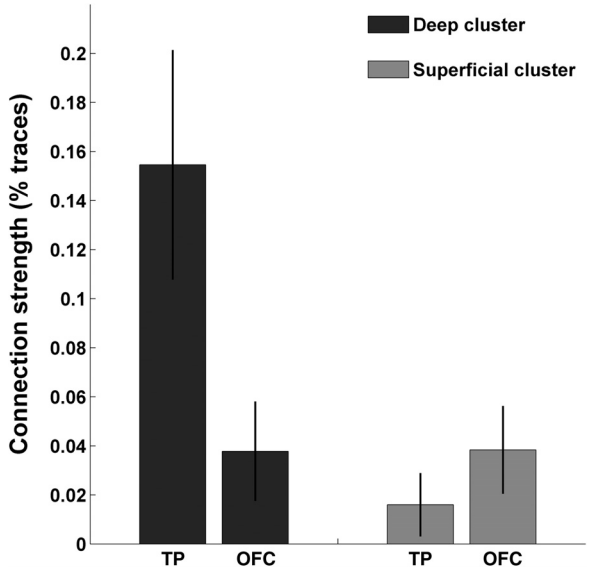

Figure 5. We determined the average connection likelihood from each amygdala cluster to each of the two target subregions. Here, we show the average percentage of traces arriving at each target region for dataset 2, where connections from the deep cluster are shown in blue, and connections from the superficial cluster in red. The interaction shown here is significant at $p < 0.05$.

with each of the two target subregions (Behrens et al., 2003a). These values were extracted, averaged across each cluster, and analyzed in a 2 (seed) × 2 (target) × 2 (hemisphere) ANOVA. Data are displayed as average percentage of traces arriving at the target region.

Results

In a first analysis where *k*-means clustering did not take into account voxel position, 98.7 ± 1.7% (dataset 1, mean ± SD) and 98.2 ± 3.4% (dataset 2) of voxels were grouped into two spatially contiguous clusters across the group, as illustrated in Figure 1 in a representative individual; the remaining voxels did not spatially connect to the cluster to which they were assigned. For our final analysis, voxel position was part of the clustering algorithm and ensured that 99.9 ± 0.4% and 99.9 ± 0.2% of voxels were assigned to contiguous clusters. In all amygdalae, we consistently identified a more anterior/inferior/lateral (cluster 1) and a more posterior/superior/medial cluster (cluster 2), with mean volumes of 634 ± 89 mm^3 and 735 ± 191 mm^3 for dataset 1, and 474 ± 100 mm^3 and 582 ± 161 mm^3 for dataset 2. As group probability maps in Figure 2 show, these clusters correspond to the anatomical location of deep and superficial nuclei. Figure 3 illustrates the morphological relations in a three-dimensional view of maximum group probability maps for the two samples, in sample-specific group space.

Figure 4 shows maximum group probability maps, across each dataset, that determine whether any target voxel has relatively stronger connections to one or other seed cluster, as identified by the clustering algorithm. That is, for each target voxel we determined whether in the clustering procedure it contributed more to connections with cluster 1 or cluster 2, and these binary images were then aligned and overlaid for all participants. It can be seen that, across the group, the OFC has stronger connections with putative superficial nucleus subgroup, consistent with the animal literature, while TP has more connections with the putative deep nuclei. This is particularly evident in the high quality dataset 2.

This pattern of result could be confirmed when we separately analyzed connection strength of the seed clusters with individual target subregions in a 2 (seed) × 2 (target) × 2 (hemisphere) ANOVA. There were no effects involving hemisphere in either of the two datasets. In dataset 1, TP had much stronger connections to both clusters than OFC ($F_{1, 15} = 49.3$; $p < 0.001$), and cluster 1 had stronger connections than cluster 2 ($F_{1, 15} = 9.5$; $p < 0.01$). A significant cluster × target interaction ($F_{1, 15} = 8.8$; $p < 0.01$) revealed differential connections of each cluster with the two targets, respectively. This effect was reflected in the ratio of connections to the two target regions which were ~9:1 in favor of the TP for cluster 1, but only 6:1 in favor of the TP for cluster 2. Dataset 2 revealed an even clearer pattern where both targets had similar connections overall ($F_{1, 7} = 1.5$; NS), cluster 1 had stronger connections overall than cluster 2 ($F_{1, 7} = 14.5$; $p < 0.01$), and the differential connections were reflected in a significant cluster × target interaction ($F_{1, 7} = 10.8$; $p < 0.05$). The connection ratios to the target regions were 4:1 in favor of TP for cluster 1, and 2.4:1 in favor of OFC for cluster 2, as shown in Figure 5.

Discussion

We investigated *in vivo* the connection profile of amygdala subregions with the lateral OFC and TP using diffusion weighted imaging and probabilistic fiber tracking. In the absence of an existing method to differentiate amygdala subregions using *in*

vivo magnetic resonance images we employed clustering methods to separate distinct amygdala regions based on differences in their connectivity profile. This method is blind to the labeling of cortical regions as OFC and TP and takes into account the whole target region.

Two key findings emerged. First, we show that it is possible to robustly distinguish two amygdala subregions based on their connectivity profile. Furthermore, these regions consist of spatially contiguous voxel groups, and their anatomical location shows a high degree of face validity in their correspondence to superficial and deep amygdala nuclear groups. Second, we demonstrate that this separation is dependent on connections to individual cortical subregions, namely OFC and TP, such that the deep cluster connects more strongly to TP, and the superficial cluster connects more strongly to OFC. This is in keeping with tract tracing studies in non-human primates that provide evidence that lateral OFC has connections to all superficial nuclei and TP has connections to lateral, basal, and accessory basal nuclei (McDonald, 1998). Our result suggests that these findings can be extrapolated to humans, and additionally allow for a quantitative description of connection likelihood, as opposed to qualitative or semiquantitative tract tracing techniques.

To the best of our knowledge, this is the first report detailing *in vivo* cortical connections to amygdala subregions. Previous reports have focused on connections of the amygdala as a whole (Bracht et al., 2009). The wider importance of our findings is that ideas such that amygdala-prefrontal connections influence associative learning (Cohen et al., 2008) and distinct aspects of emotional processes (Kim and Whalen, 2009) can now be tested more rigorously. Indeed, given the putative differential role of deep and superficial amygdala nucleus in learning and emotion, it should now be possible to ascribe greater anatomical specificity to human *in vivo* data.

To reveal amygdalo-cortical connections, the technique presented here involves a data driven *in vivo* segmentation of the amygdala based on connectivity profiles, an approach blind to target region location and therefore unbiased. Such segmentation can be used in a wide range of applications, such as guiding analysis and interpretation of functional imaging studies. Parcellating the amygdala into meaningful subregions *in vivo*, using magnetic resonance images, has heretofore presented a major methodological challenge due to its small size and macroscopically homogenous appearance. A recent methodological paper has proposed a method to find clusters within the amygdala based on diffusion direction in gray matter (Solano-Castiella et al., 2010). Our approach is different and relies on exploiting the connectivity of individual amygdala subregions.

Human neuroimaging studies have often investigated neural activity in the amygdala across a range of experimental contexts, but these studies typically do not provide precision in relation to anatomy rendering it difficult to localize activation patterns. A few functional magnetic resonance imaging (fMRI) studies have tried to delineate responses in nucleus groups by manual drawing of regions of interest corresponding to superficial and deep amygdala in native space (Etkin et al., 2004), or using masks based on cytoarchitectonic probability maps in MNI space (Ball et al., 2007; Goossens et al., 2009; Roy et al., 2009). The limitation of the former approach is the fact that manual delineation of individual amygdala nuclei on T1-weighted images has not yet been described in the anatomical or radiological literature. The use of probability maps on the other hand has a strong theoretical justification but this approach does not account for individual variation in anatomy such that there is a large uncertainty associated with these findings. We suggest our approach provides a more nuanced means to define amygdala regions of interest for functional neuroimaging studies and can be used to elucidate, with greater precision, the role of these subregions in higher primates.

While our finding of differential amygdala connectivity is robust across two datasets, the use of these connectivity profiles to identify amygdala subregions has some noteworthy limitations. In particular, across the group there was much less variation of cluster location and connections with the cortical masks in dataset 2 where diffusion weighted images were acquired four times instead of twice. This points to a potentially low signal-to-noise ratio in the diffusion weighted data, and possibly also to susceptibility artifacts. The use of several acquisitions and careful artifact correction is likely to be of importance for such data, particularly in regions such as the amygdala which are small in extent and located close to susceptibility interfaces. The same reasoning applies to the manual delineation of the amygdala as a whole which we propose is more accurate in the higher quality T1 images of dataset 2 as apparent in smaller volumes. Although we propose that the two clusters map on to deep and superficial nuclear collections, we accept that it is difficult to equate the clusters with exact nuclear groups. Caution is warranted based on animal histology, where the dorsal lateral and magnocellular basal nuclei might connect both to OFC and TP (McDonald, 1998) such that the clustering algorithm might group them into either cluster. Consequently, there is a possibility that the extent of the superficial cluster might be overestimated. Furthermore, the low resolution of our current diffusion data does not allow any insight into the fine divisions between amygdala nuclei within each nuclear group. Finally, if parcellation of amygdala nuclei is the main goal, it is likely to prove useful to include more target areas, especially if high image quality allows reliable tractography for areas with weak, but nonetheless specific, amygdala connections, such as the medial prefrontal cortex.

To summarize, we show that the amygdala can be grouped into two distinct subregions based on their distinct cortical connection profiles. The location of these subgroups is consistent with deep and superficial amygdala nuclei, and their connections are broadly consistent with predictions from monkey tracer studies. Thus, histological findings from non-human primates concerning the connectivity of amygdala nuclei can be extrapolated to humans. Our approach provides a potential method that can be exploited to provide a more rigorous functional anatomy of the amygdala.

References

Adolphs R, Spezio M (2006) Role of the amygdala in processing visual social stimuli. Prog Brain Res 156:363–378.

Andersson JL, Skare S, Ashburner J (2003) How to correct susceptibility distortions in spin-echo echo-planar images: application to diffusion tensor imaging. Neuroimage 20:870–888.

Ashburner J (2007) A fast diffeomorphic image registration algorithm. Neuroimage 38:95–113.

Ball T, Rahm B, Eickhoff SB, Schulze-Bonhage A, Speck O, Mutschler I (2007) Response properties of human amygdala subregions: evidence based on functional MRI combined with probabilistic anatomical maps. PLoS One 2:e307.

Basser PJ, Mattiello J, LeBihan D (1994a) Estimation of the effective self-diffusion tensor from the NMR spin echo. J Magn Reson B 103:247–254.

Basser PJ, Mattiello J, LeBihan D (1994b) MR diffusion tensor spectroscopy and imaging. Biophys J 66:259–267.

Beaulieu C, Allen PS (1994) Determinants of anisotropic water diffusion in nerves. Magn Reson Med 31:394–400.

Behrens TE, Johansen-Berg H (2005) Relating connectional architecture to

grey matter function using diffusion imaging. Philos Trans R Soc Lond B Biol Sci 360:903–911.

Behrens TE, Johansen-Berg H, Woolrich MW, Smith SM, Wheeler-Kingshott CA, Boulby PA, Barker GJ, Sillery EL, Sheehan K, Ciccarelli O, Thompson AJ, Brady JM, Matthews PM (2003a) Non-invasive mapping of connections between human thalamus and cortex using diffusion imaging. Nat Neurosci 6:750–757.

Behrens TE, Woolrich MW, Jenkinson M, Johansen-Berg H, Nunes RG, Clare S, Matthews PM, Brady JM, Smith SM (2003b) Characterization and propagation of uncertainty in diffusion-weighted MR imaging. Magn Reson Med 50:1077–1088.

Behrens TE, Berg HJ, Jbabdi S, Rushworth MF, Woolrich MW (2007) Probabilistic diffusion tractography with multiple fibre orientations: what can we gain? Neuroimage 34:144–155.

Bracht T, Tüscher O, Schnell S, Kreher B, Rüsch N, Glauche V, Lieb K, Ebert D, Il'yasov KA, Hennig J, Weiller C, van Elst LT, Saur D (2009) Extraction of prefronto-amygdalar pathways by combining probability maps. Psychiatry Res 174:217–222.

Carmichael ST, Price JL (1995) Limbic connections of the orbital and medial prefrontal cortex in macaque monkeys. J Comp Neurol 363:615–641.

Chang LC, Jones DK, Pierpaoli C (2005) RESTORE: robust estimation of tensors by outlier rejection. Magn Reson Med 53:1088–1095.

Cohen MX, Elger CE, Weber B (2008) Amygdala tractography predicts functional connectivity and learning during feedback-guided decision-making. Neuroimage 39:1396–1407.

Dale AM, Fischl B, Sereno MI (1999) Cortical surface-based analysis. I. Segmentation and surface reconstruction. Neuroimage 9:179–194.

Davis M, Whalen PJ (2001) The amygdala: vigilance and emotion. Mol Psychiatry 6:13–34.

Deichmann R, Good CD, Turner R (2002) RF inhomogeneity compensation in structural brain imaging. Magn Reson Med 47:398–402.

Deichmann R, Schwarzbauer C, Turner R (2004) Optimisation of the 3D MDEFT sequence for anatomical brain imaging: technical implications at 1.5 and 3 T. Neuroimage 21:757–767.

Etkin A, Klemenhagen KC, Dudman JT, Rogan MT, Hen R, Kandel ER, Hirsch J (2004) Individual differences in trait anxiety predict the response of the basolateral amygdala to unconsciously processed fearful faces. Neuron 44:1043–1055.

Fischl B, Sereno MI, Dale AM (1999) Cortical surface-based analysis. II: Inflation, flattening, and a surface-based coordinate system. Neuroimage 9:195–207.

Fischl B, van der Kouwe A, Destrieux C, Halgren E, Ségonne F, Salat DH, Busa E, Seidman LJ, Goldstein J, Kennedy D, Caviness V, Makris N, Rosen B, Dale AM (2004) Automatically parcellating the human cerebral cortex. Cereb Cortex 14:11–22.

Freese JL, Amaral DG (2009) Neuroanatomy of the primate amygdala. In: The human amygdala (Whalen PJ, Phelps EA, eds), pp 3–42. New York: Guilford.

Goossens L, Kukolja J, Onur OA, Fink GR, Maier W, Griez E, Schruers K, Hurlemann R (2009) Selective processing of social stimuli in the superficial amygdala. Hum Brain Mapp 30:3332–3338.

Gray JA, McNaughton N (2000) The neuropsychology of anxiety: an enquiry into the functions of the septohippocampal system. Oxford, UK: Oxford UP.

Hartigan JA (1975) Clustering algorithms. New York: Wiley.

Howarth C, Hutton C, Deichmann R (2006) Improvement of the image quality of T1-weighted anatomical brain scans. Neuroimage 29:930–937.

Johansen-Berg H, Behrens TE, Robson MD, Drobnjak I, Rushworth MF, Brady JM, Smith SM, Higham DJ, Matthews PM (2004) Changes in connectivity profiles define functionally distinct regions in human medial frontal cortex. Proc Natl Acad Sci U S A 101:13335–13340.

Kim MJ, Whalen PJ (2009) The structural integrity of an amygdala-prefrontal pathway predicts trait anxiety. J Neurosci 29:11614–11618.

LeDoux JE (2000) Emotion circuits in the brain. Annu Rev Neurosci 23:155–184.

Mai JK, Paxinos G, Voss T (2008) Atlas of the human brain. New York: Elsevier.

McDonald AJ (1998) Cortical pathways to the mammalian amygdala. Prog Neurobiol 55:257–332.

Nagy Z, Weiskopf N, Alexander DC, Deichmann R (2007) A method for improving the performance of gradient systems for diffusion-weighted MRI. Magn Reson Med 58:763–768.

Pitkänen A (2000) Connectivity of the rat amygdaloid complex. In: The amygdala—a functional analysis (Aggleton JP, ed), pp 31–116. Oxford: Oxford UP.

Reese TG, Heid O, Weisskoff RM, Wedeen VJ (2003) Reduction of eddy-current-induced distortion in diffusion MRI using a twice-refocused spin echo. Magn Reson Med 49:177–182.

Roy AK, Shehzad Z, Margulies DS, Kelly AM, Uddin LQ, Gotimer K, Biswal BB, Castellanos FX, Milham MP (2009) Functional connectivity of the human amygdala using resting state fMRI. Neuroimage 45:614–626.

Sander D, Grafman J, Zalla T (2003) The human amygdala: An evolved system for relevance detection. Rev Neurosci 14:303–316.

Ségonne F, Dale AM, Busa E, Glessner M, Salat D, Hahn HK, Fischl B (2004) A hybrid approach to the skull stripping problem in MRI. Neuroimage 22:1060–1075.

Solano-Castiella E, Anwander A, Lohmann G, Weiss M, Docherty C, Geyer S, Reimer E, Friederici AD, Turner R (2010) Diffusion tensor imaging segments the human amygdala in vivo. Neuroimage 49:2958–2965.

Tomassini V, Jbabdi S, Klein JC, Behrens TE, Pozzilli C, Matthews PM, Rushworth MF, Johansen-Berg H (2007) Diffusion-weighted imaging tractography-based parcellation of the human lateral premotor cortex identifies dorsal and ventral subregions with anatomical and functional specializations. J Neurosci 27:10259–10269.

Zald DH (2003) The human amygdala and the emotional evaluation of sensory stimuli. Brain Res Rev 41:88–123.